Received 11 January; accepted 20 February 2002.

1. Savill, J. & Fadok, V. Corpse clearance defines the meaning of cell death. *Nature* **407,** 784–788 (2000).
2. Platt, N., da Silva, R. P. & Gordon, S. Recognizing death: the phagocytosis of apoptotic cells. *Trends Cell Biol.* **8,** 365–372 (1998).
3. Stubbs, J. D. *et al.* cDNA cloning of a mouse mammary epithelial cell surface protein reveals the existence of epidermal growth factor-like domains linked to factor VIII-like sequences. *Proc. Natl Acad. Sci. USA* **87,** 8417–8421 (1990).
4. Oshima, K. *et al.* Lactation-dependent expression of an mRNA splice variant with an exon for a multiply O-glycosylated domain of mouse milk fat globule glycoprotein MFG-E8. *Biochem. Biophys. Res. Commun.* **254,** 522–528 (1999).
5. McIlroy, D. *et al.* An auxiliary mode of apoptotic DNA fragmentation provided by phagocytes. *Genes Dev.* **14,** 549–558 (2000).
6. Bowman, E. J., Siebers, A. & Altendorf, K. Bafilomycins: a class of inhibitors of membrane ATPases from microorganisms, animal cells, and plant cells. *Proc. Natl Acad. Sci. USA* **85,** 7972–7976 (1988).
7. Koopman, G. *et al.* Annexin V for flow cytometric detection of phosphatidylserine expression on B cells undergoing apoptosis. *Blood* **84,** 1415–1420 (1994).
8. Hynes, R. O. Integrins: versatility, modulation, and signalling in cell adhesion. *Cell* **69,** 11–25 (1992).
9. Fadok, V. A., Bratton, D. L., Frasch, S. C., Warner, M. L. & Henson, P. M. The role of phosphatidylserine in recognition of apoptotic cells by phagocytes. *Cell Death Differ.* **5,** 551–562 (1998).
10. Nakano, T. *et al.* Cell adhesion to phosphatidylserine mediated by a product of growth arrest-specific gene 6. *J. Biol. Chem.* **272,** 29411–29414 (1997).
11. Savill, J., Hogg, N., Ren, Y. & Haslett, C. Thrombospondin cooperates with CD36 and the vitronectin receptor in macrophage recognition of neutrophils undergoing apoptosis. *J. Clin. Invest.* **90,** 1513–1522 (1992).
12. Ogden, C. A. *et al.* C1q and mannose binding lectin engagement of cell surface calreticulin and CD91 initiates macropinocytosis and uptake of apoptotic cells. *J. Exp. Med.* **194,** 781–795 (2001).
13. Fadok, V. A. *et al.* Different populations of macrophages use either the vitronectin receptor or the phosphatidylserine receptor to recognize and remove apoptotic cells. *J. Immunol.* **149,** 4029–4035 (1992).
14. Emoto, K., Toyama-Sorimachi, N., Karasuyama, H., Inoue, K. & Umeda, M. Exposure of phosphatidylethanolamine on the surface of apoptotic cells. *Exp. Cell Res.* **232,** 430–434 (1997).
15. Blankenberg, F. G. *et al.* In vivo detection and imaging of phosphatidylserine expression during programmed cell death. *Proc. Natl Acad. Sci. USA* **95,** 6349–6354 (1998).
16. Fadok, V. A., de Cathelineau, A., Daleke, D. L., Henson, P. M. & Bratton, D. L. Loss of phospholipid asymmetry and surface exposure of phosphatidylserine is required for phagocytosis of apoptotic cells by macrophages and fibroblasts. *J. Biol. Chem.* **276,** 1071–1077 (2001).
17. Rigotti, A., Acton, S. L. & Krieger, M. The class B scavenger receptors SR-BI and CD36 are receptors for anionic phospholipids. *J. Biol. Chem.* **270,** 16221–16224 (1995).
18. Savill, J., Dransfield, I., Hogg, N. & Haslett, C. Vitronectin receptor-mediated phagocytosis of cells undergoing apoptosis. *Nature* **343,** 170–173 (1990).
19. Albert, M. L., Sauter, B. & Bhardwaj, N. Dendritic cells acquire antigen from apoptotic cells and induce class I-restricted CTLs. *Nature* **392,** 86–89 (1998).
20. Hengartner, M. O. Apoptosis: corralling the corpses. *Cell* **104,** 325–328 (2001).
21. Fadok, V. A. *et al.* A receptor for phosphatidylserine-specific clearance of apoptotic cells. *Nature* **405,** 85–90 (2000).
22. Scott, R. S. *et al.* Phagocytosis and clearance of apoptotic cells is mediated by MER. *Nature* **411,** 207–211 (2001).
23. Wilde, C. J., Knight, C. H. & Flint, D. J. Control of milk secretion and apoptosis during mammary involution. *J. Mamm. Gland Biol. Neoplasia* **4,** 129–136 (1999).
24. Fadok, V. A. Clearance: the last and often forgotten stage of apoptosis. *J. Mamm. Gland Biol. Neoplasia* **4,** 203–211 (1999).
25. Wada, J. *et al.* Cloning of mouse integrin α_V cDNA and role of the α_V-related matrix receptors in metanephric development. *J. Cell. Biol.* **132,** 1161–1176 (1996).
26. McHugh, K. P., Kitazawa, S., Teitelbaum, S. L. & Ross, F. P. Cloning and characterization of the murine β(3) integrin gene promoter: identification of an interleukin-4 responsive element and regulation by STAT-6. *J. Cell Biochem.* **81,** 320–332 (2001).
27. Taylor, P. R. *et al.* A hierarchical role for classical pathway complement proteins in the clearance of apoptotic cells in vivo. *J. Exp. Med.* **192,** 359–366 (2000).
28. Kawane, K. *et al.* Requirement of DNase II for definitive erythropoiesis in the mouse fetal liver. *Science* **292,** 1546–1549 (2001).
29. Iwamatsu, A. & Yoshida-Kubomura, N. Systematic peptide fragmentation of polyvinylidine difluoride (PVDF)-immobilized proteins prior to microsequencing. *J. Biochem. (Tokyo)* **120,** 29–34 (1996).
30. Andersen, M. H., Berglund, L., Rasmussen, J. T. & Petersen, T. E. Bovine PAS-6/7 binds $\alpha_v\beta_5$ integrins and anionic phospholipids through two domains. *Biochemistry* **36,** 5441–5446 (1997).

Supplementary Information accompanies the paper on *Nature*'s website (http://www.nature.com).

Acknowledgements

We thank T. Kitamura for the retrovirus expression system, Y. Seto for maintaining the mice, and S. Aoyama for secretarial assistance. This work was supported in part by Grants-in-Aid from the Ministry of Education, Science, Sports and Culture in Japan.

Competing interests statement

The authors declare that they have no competing financial interests.

Correspondence and requests for materials should be addressed to S. N. (e-mail: nagata@genetic.med.osaka-u.ac.jp).

Dissection of COPI and Arf1 dynamics *in vivo* and role in Golgi membrane transport

John F. Presley*†, Theresa H. Ward*, Andrea C. Pfeifer*, Eric D. Siggia‡, Robert D. Phair§ & Jennifer Lippincott-Schwartz*

* *Cell Biology and Metabolism Branch, National Institute of Child Health and Human Development, National Institutes of Health, Bethesda, Maryland 20892, USA*

‡ *Center for Studies in Physics and Biology, The Rockefeller University, New York, New York 10021, USA*

§ *BioInformatics Services, Rockville, Maryland 20854, USA*

Cytosolic coat proteins that bind reversibly to membranes have a central function in membrane transport within the secretory pathway[1,2]. One well-studied example is COPI or coatomer, a heptameric protein complex that is recruited to membranes by the GTP-binding protein Arf1. Assembly into an electron-dense coat then helps in budding off membrane to be transported between the endoplasmic reticulum (ER) and Golgi apparatus[2]. Here we propose and corroborate a simple model for coatomer and Arf1 activity based on results analysing the distribution and lifetime of fluorescently labelled coatomer and Arf1 on Golgi membranes of living cells. We find that activated Arf1 brings coatomer to membranes. However, once associated with membranes, Arf1 and coatomer have different residence times: coatomer remains on membranes after Arf1-GTP has been hydrolysed and dissociated. Rapid membrane binding and dissociation of coatomer and Arf1 occur stochastically, even without vesicle budding. We propose that this continuous activity of coatomer and Arf1 generates kinetically stable membrane domains that are connected to the formation of COPI-containing transport intermediates. This role for Arf1/coatomer might provide a model for investigating the behaviour of other coat protein systems within cells.

To study coatomer dynamics *in vivo*, variants of green fluorescent protein (GFP), namely enhanced GFP (EGFP) and enhanced yellow fluorescent protein (EYFP), were fused to the carboxy terminus of the ϵCOP subunit of coatomer (ϵCOP–GFP or ϵCOP–YFP) and expressed in *ldlF* cells, which contain a mutated ϵCOP that at 40 °C is degraded, causing coatomer inactivity and growth inhibition[3]. The cells grew indefinitely at 40 °C (Fig. 1a), indicating that ϵCOP–GFP could substitute functionally for endogenous ϵCOP in coatomer complexes in these cells. Subsequent experiments were performed with stable *ldlF* cell lines expressing ϵCOP–GFP (or ϵCOP–YFP) that were selected by continuous growth at 40 °C unless indicated otherwise. ϵCOP–GFP in these cells localized in a manner that was indistinguishable from that of endogenous coatomer detected by antibody staining of βCOP (Fig. 1b). Biochemical (Supplementary Information) and kinetic (see below) analyses revealed that most ϵCOP–GFP molecules were stably assembled into coatomer complexes that underwent binding and dissociation from membranes.

The identity and behaviour of coatomer-containing membranes, assessed by ϵCOP–YFP labelling, were studied in dual-colour time-lapse experiments in cells co-expressing cyan fluorescent protein (CFP)-tagged secretory cargo markers. ϵCOP–YFP was present on juxtanuclear Golgi membranes, as well as on ER-to-Golgi (anterograde) transport intermediates containing vesicular stomatitis virus ts045 G protein (VSVG) tagged with CFP in cells shifted from

† Present address: Department of Anatomy and Cell Biology, McGill University, Montreal, Quebec, Canada.

40 °C to 15 °C (Fig. 1c)[4]. On being warmed to 32 °C, the anterograde intermediates moved as globular or tubular shapes towards the Golgi complex, with ϵCOP–YFP remaining localized on their surfaces (Fig. 1d, e). ϵCOP–YFP was only weakly associated with presumptive retrograde, Golgi-to-ER, transport intermediates, which appeared as Golgi tubule extensions when immunolabelled with the ERGIC53 homologue p58 (not shown), an ER/Golgi cycling molecule[5], or when co-stained with p58–CFP (Fig. 1f). No small fluorescent objects with the predicted size of vesicles (that is, one pixel) were observed moving out from any of these structures (Supplementary Information). These findings are consistent with previous reports of coatomer distribution within living cells[6,7].

To measure how rapidly coatomer dissociates from Golgi membranes, we performed fluorescence loss in photobleaching (FLIP) experiments[8]. On repeated bleaching outside the Golgi, all cellular ϵCOP–GFP fluorescence was lost in a few minutes (Fig. 2a), indicating that coatomer resides on Golgi membranes only transiently before dissociating and exchanging with cytoplasmic pools. To determine the rate at which coatomer rebinds to Golgi membranes, we selectively photobleached the Golgi and then watched for fluorescence recovery after photobleaching (FRAP)[8]. The prebleach, Golgi-to-cytoplasmic fluorescence ratio (that is, 40:60) recovered exponentially with a half-time ($t_{1/2}$) of 35 s (Fig. 2b, c) and was not affected by microtubule disruption (which inhibits the movement of anterograde transport intermediates) (not shown). This indicated that recovery was mediated not by delivery via anterograde intermediates but by exchange between Golgi-bound and freely mobile cytoplasmic pools of coatomer. FRAP experiments examining ϵCOP–GFP dynamics on anterograde intermediates revealed that ϵCOP–GFP also rapidly exchanged on and off these structures (Fig. 2d), whether or not they were moving, and at a rate similar to that at the Golgi complex. In cells co-expressing the active GTP-bound form of Arf1[Q71L] that is unable to hydrolyse GTP[9], or in cells treated with GTP-γS (not shown), ϵCOP–GFP became irreversibly bound to membranes and no fluorescence recovery occurred during FRAP (Fig. 2c, e). These results indicate that coatomer dissociation from membranes *in vivo* occurs rapidly and is dependent on Arf1-GTP hydrolysis[10].

To determine whether coatomer dissociation from membranes coincides with Arf1-GTP hydrolysis, we examined by FRAP the

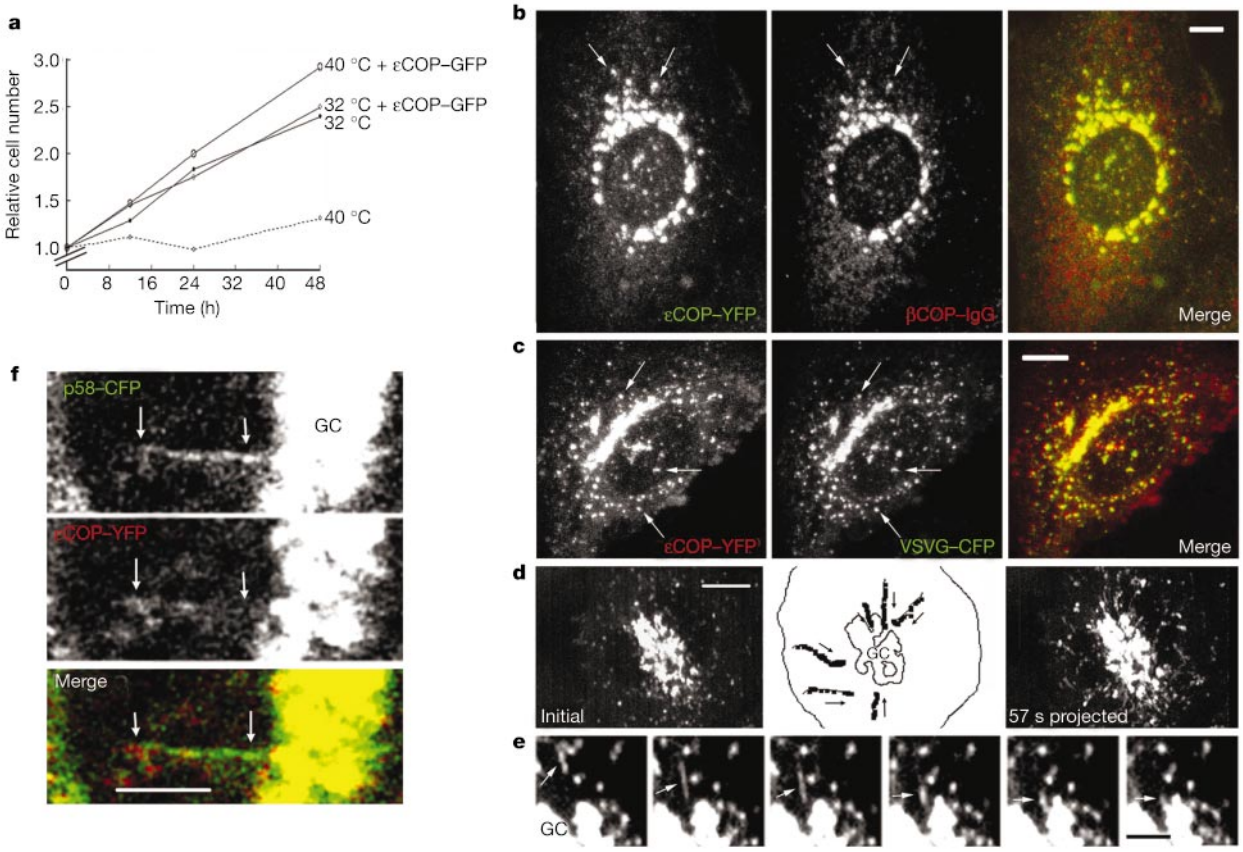

Figure 1 Incorporation of ϵCOP–GFP into functional coatomer complexes and their distribution. **a**, Growth rate (cell number relative to initial cell number with time) at 32 or 40 °C in untreated *ldlF* cells and *ldlF* cells expressing ϵCOP–GFP by transient transfection. **b**, Co-localization of ϵCOP–GFP (left) and βCOP stained with anti-βCOP antibody (generated from the EAGE peptide) single-letter amino-acid codes) in βCOP) and rhodamine secondary antibody (middle) in an *ldlF* cell stably expressing ϵCOP–GFP. Merged image (right) shows co-localization (yellow) of the markers in Golgi and peripheral structures (see arrows). Scale bar, 5 μM. **c**, *ldlF* cells stably expressing ϵCOP–YFP were transfected with VSVG–CFP and incubated at 40 °C to accumulate VSVG–CFP in the ER. The temperature was lowered to 15 °C for 3 h to accumulate VSVG–CFP in ER-to-Golgi transport intermediates. Extensive co-localization (yellow, merged image) of the two markers was found in peripheral (arrowed) and juxtanuclear structures. Scale bar, 5 μM. **d**, Inward movement of peripheral ϵCOP–GFP-containing structures in *ldlF* cells stably expressing ϵCOP–GFP. Shown are the initial image of the time series (left), several representative tracks taken by peripheral structures during the time series (middle), and a maximum-value projection of the entire time series (acquired at two images s^{-1} for 57 s) showing paths taken by translocating structures (right). Scale bar, 5 μM. (See Quicktime movie in Supplementary Information.) **e**, Area near the Golgi complex (GC) from the time series in **d** illustrating tubulation of a ϵCOP–GFP labelled structure as it translocates towards the Golgi complex. Scale bar, 2 μM. **f**, Still frame from a time sequence in an NRK cell expressing p58–CFP (top) and ϵCOP–YFP (middle). The merged image (bottom) shows only low levels of ϵCOP–YFP on p58–CFP-containing Golgi tubules (arrowed). Scale bar, 5 μM.

kinetics of Arf1 membrane association and dissociation (which is mediated by GTP binding and hydrolysis[10]) by using a GFP-tagged Arf1 (ref. 11) (Arf1–GFP). Addition of the GFP tag did not alter any of Arf1's essential roles: Arf1–GFP functionally replaced the endogenous copy of *ARF1* in a Δ*arf2* yeast strain, and when expressed as a GTP-locked form (that is, Arf1[Q71L]–GFP) it could protect endogenous COPI from membrane release in the presence of brefeldin A (BFA) (Supplementary Information, Figs S1 and S2). During FRAP, exchange of bleached Arf1–GFP in the Golgi with unbleached Arf1–GFP in the cytoplasm occurred rapidly (Fig. 3a), was not limited by cytoplasmic diffusion of Arf1–GFP and was dependent on GTP hydrolysis because exchange did not occur in cells injected with GTP-γS (not shown). Recovery was faster than that reported previously for Arf1–GFP[11] because of differences in FRAP conditions (Supplementary Information). Because the $t_{1/2}$ for recovery of Arf1–GFP (15 s) was significantly faster than for coatomer (35 s) measured under similar conditions, the data indicated that coatomer is stabilized on membranes for additional periods after Arf1 undergoes GTP hydrolysis and dissociation.

We visualized Arf1 and coatomer dissociation from membranes directly in cells co-expressing Arf1–CFP and ϵCOP–YFP treated with BFA[10]. BFA blocks the binding of Arf1 to membranes and the recruitment of coatomer by Arf1 (ref. 12), allowing the dissociation of Arf1 and coatomer to be observed in the absence of rebinding. On treatment with BFA, Arf1–CFP and ϵCOP–YFP rapidly dissociated from Golgi membranes before Golgi disassembly (Fig. 3b). The half-time for dissociation of Arf1–CFP (13 s) was significantly faster than that for ϵCOP–YFP (30 s). Similar half-times were measured in cells expressing the chimaeras individually, and with Arf1 tagged with the small haemagglutinin epitope (HA–Arf1), a widely used Arf1 reporter[13] (Supplementary Information, Fig. S3), supporting the conclusion that Arf1 and coatomer dissociate independently from Golgi membranes.

We used FRAP or treatment with BFA to examine the effect of coatomer on the rate of dissociation of Arf1–GFP from the Golgi[14,15] in two situations: when coatomer is irreversibly membrane-bound by treatment with AlF (ref. 16), an activator of trimeric G proteins[17]; and after the depletion of coatomer from cells. Treatment with a range of AlF concentrations had no major effect on the FRAP kinetics of Arf1–GFP (Fig. 3f, g) despite irreversible binding of ϵCOP–GFP to membranes (Fig. 3d, e) (see also Supplementary Information, Fig. S4). Moreover, coatomer depletion (Fig. 4a) had no effect on the FRAP recovery rate of Arf1–GFP (not shown) or on the release rate of Arf1–GFP from the Golgi after treatment with BFA (Fig. 4b). Thus, whether coatomer is stabilized on or depleted from membranes has no detectable effect on the GAP-mediated, GTP-hydrolysis-dependent membrane release of Arf1–GFP *in vivo*.

On the basis of the above results and previous data we formulated a simple model of activity and turnover of Arf1 and coatomer on membrane (Fig. 4c). The model explicitly uncouples Arf1 and coatomer release from membranes and posits no feedback from coatomer to Arf1. It encompasses the following six processes: (1) binding of cytoplasmic Arf1 to Golgi membranes and activation by guanine nucleotide exchange[18,19], which is inhibited by BFA[12]; (2) recruitment of cytoplasmic coatomer to Golgi membranes by binding to activated Arf1 (ref. 20); (3) interaction of activated Arf1 with alternative effector molecules in Golgi membranes[21]; (4) GTPase-activating protein (GAP)-mediated hydrolysis of GTP bound to Arf1 (ref. 22) in either coatomer[14] or alternative effector complexes[21] with the concomitant release of Arf1–GDP to the cytoplasm, while coatomer remains Golgi-associated; (5) binding of coatomer to membrane cargo, soluble-cargo receptors or other Golgi proteins[23,24]; and (6) uncoating or release of coatomer from Golgi membranes to cytoplasm, which is inhibited by AlF (ref. 16).

To test this model quantitatively we formulated it on the basis of standard principles of chemical kinetics, with each process contributing terms to a system of differential equations (Supplementary

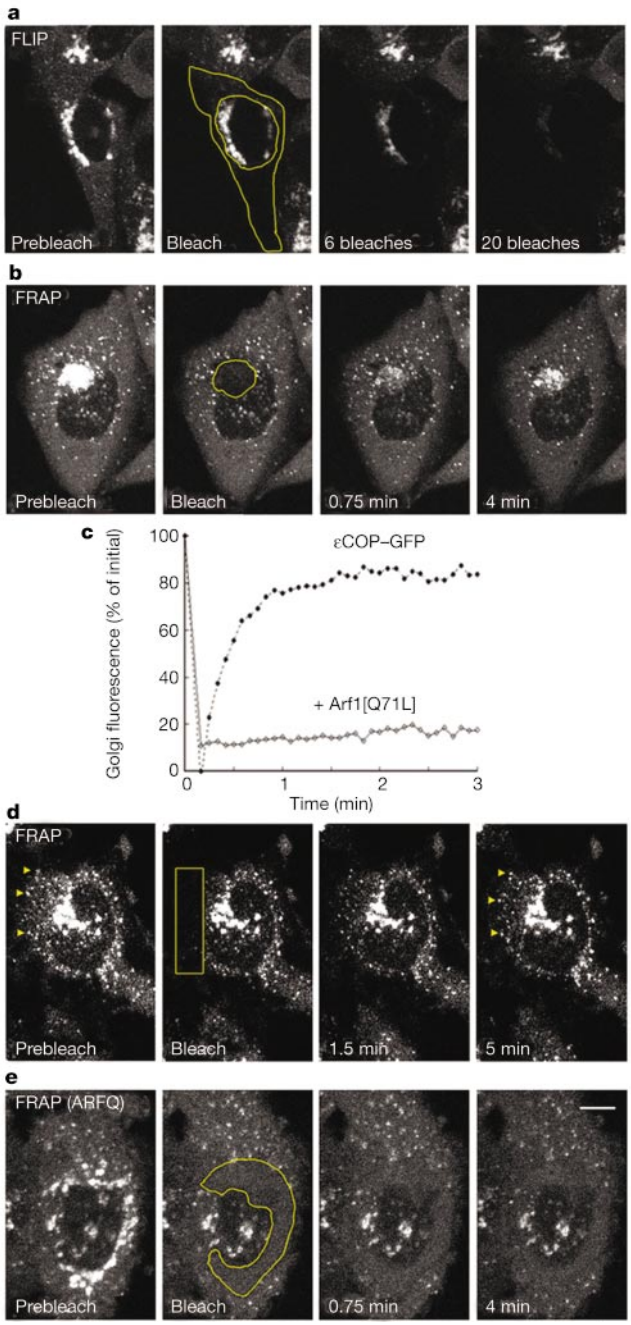

Figure 2 Kinetics of COPI binding to and dissociation from Golgi and ER-to-Golgi transport intermediates in *ldlF* cells stably expressing ϵCOP–GFP. **a**, Repeated photobleaching (FLIP) (one bleach every 15 s) of the cytoplasm (defined by the area between the two yellow lines). **b**, Golgi-FRAP. An initial prebleach image was taken (prebleach), then the Golgi region of interest (indicated by yellow outline) was bleached with high-intensity laser light. After the bleach, images were taken at 5–10-s intervals to monitor exchange between photobleached and non-bleached ϵCOP–GFP. Scale bar, 5 μM. (See Quicktime movies in Supplementary Information.) **c**, Quantification of Golgi FRAP protocol with and without co-expression of Arf1[Q71L]. **d**, FRAP of ER-to-Golgi intermediates. To prevent movement of the intermediates, cells were chilled on ice for 20 min and warmed to 37 °C in the presence of 1 μg ml^{-1} nocodazole to depolymerize microtubules. The area within the yellow box in the cell periphery was illuminated with high-intensity laser light to photobleach the fluorescent structures containing ϵCOP–GFP. Arrowheads point to ER-to-Golgi intermediates that recovered their fluorescence while remaining at the same location. (See Quicktime movies in Supplementary Information.) **e**, FRAP of an area containing the Golgi region of interest (indicated by yellow outline) in a cell microinjected 5 h previously with a plasmid coding for the GTP-bound Arf1[Q71L] mutant (ARFQ). Golgi-associated fluorescence does not recover after photobleaching, indicating that exchange between Golgi and cytoplasmic ϵCOP–GFP is inhibited in these cells.

Information). We then examined whether it could account for the Arf1–GFP and ϵCOP–GFP photobleaching data (Figs 2c and 3a) and the Arf1–CFP and ϵCOP–YFP kinetics after treatment with BFA (Fig. 3b, c) while accounting for the steady-state abundances of Arf1 and coatomer on membranes and in cytoplasm. The latter was assessed by quantification of the fluorescent images with GFP standard solutions and by western blot analysis (Supplementary Information). Significantly, we found that the model could account for all eight data sets by using the same set of parameter values (that is, rate constants). This is illustrated in Fig. 4d, by plotting the model solutions (smooth curves) on the same axes as the corresponding experimental data (dotted curves). The relevant rate constants were $0.0127\ s^{-1}$ for binding of cytoplasmic Arf1 to Golgi (process 1), 1.05×10^{-8} (molecules per cell)$^{-1}$ s^{-1} for binding of cytoplasmic

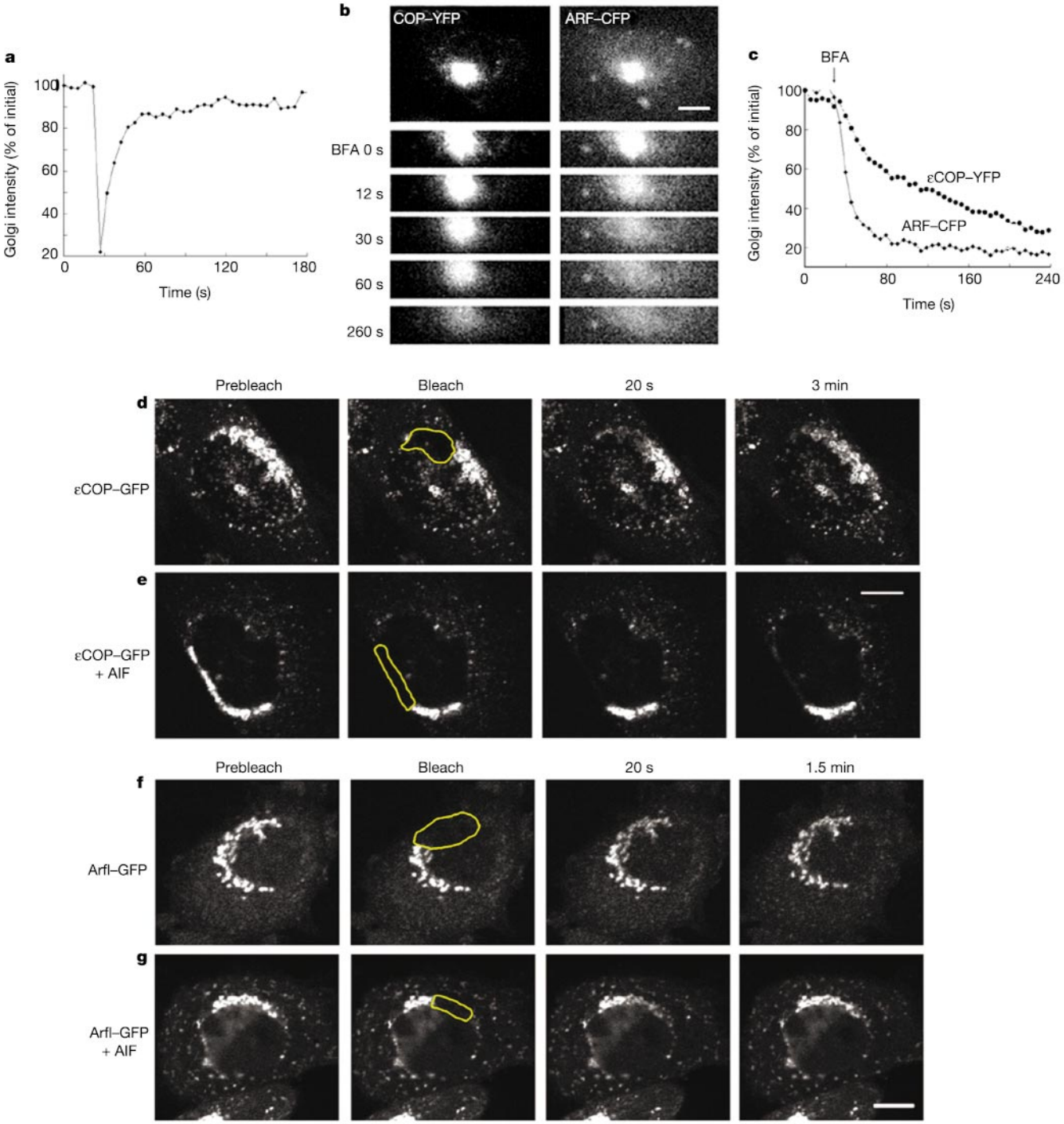

Figure 3 Golgi association–dissociation kinetics of Arf1–GFP/CFP and ϵCOP–GFP/YFP in AlF-treated or BFA-treated cells. **a**, Quantification of Golgi FRAP in CHO cell expressing Arf1-GFP. **b**, Kinetics of dissociation of ϵCOP–YFP and Arf1–CFP from Golgi membranes after the addition of BFA (5 μg ml^{-1}) in an *ldlF* cell co-expressing both proteins. **c**, Quantification of dissociation kinetics of ϵCOP–YFP and Arf1–CFP from the experiment in **b**. **d**, **e**, *ldlF* cells expressing ϵCOP–GFP were selectively photobleached within the yellow outline after no treatment (**d**) or after treatment with AlF (50 μM $AlCl_3$, 0.1 mM NaF) for 10 min (**e**). Recovery into the bleached area was monitored by imaging cells with low illumination levels. **f**, **g**, CHO cells expressing only Arf1–GFP were selectively photobleached inside the yellow line after no treatment (**f**) or after treatment with AlF for 10 min (**g**). Recovery into the bleached area was monitored by imaging cells with low illumination levels. Scale bar, 5 μM.

COPI to Golgi (process 2), 0.0384 s^{-1} for GTP hydrolysis by Golgi-bound Arf1 (process 4) and 0.0231 s^{-1} for loss of COPI from Golgi (process 6). Thus, the average residence time for coatomer on Golgi membranes is 43 s, in contrast with 26 s for Arf1. These residence times were the same whether calculated from photobleaching or from BFA-release experiments and are consistent with our current understanding that BFA inhibits solely the Arf1 exchange factor (process 1)[10,12].

We considered a simpler model in which all Arf1 used coatomer as an effector (that is, process 3 was eliminated). This model failed to account for the relative abundance of Arf1 and COPI on membrane and in cytoplasm. In another model we postulated the simultaneous release of Arf1 and coatomer to the cytoplasm, to correspond to the widespread assumption that uncoating is a consequence of Arf1-GTP hydrolysis[2]. This model could not account for the slower coatomer dynamics observed during FRAP or BFA protocols. Thus, the model shown in Fig. 4c, which simultaneously accounts for all data sets (Fig. 4d), is our current working hypothesis.

It is widely believed that coatomer binds to membranes and then polymerizes into a coat. The coat then shapes the adherent membrane into a coated bud that gives rise to a coated vesicle (Fig. 5a). The vesicle then uncoats and all accumulated coatomer is released at once[1,2]. Because of the sequential steps occurring before vesicle uncoating in this model, coatomer release should exhibit non-exponential kinetics (for example, it should show a shoulder or lag) (Supplementary Information). However, the observed release kinetics of coatomer from membranes (Fig. 4d) was exponential, leading to a possible alternative role for coatomer (Fig. 5b) in which continuous Arf1-driven binding and dissociation of coatomer serves to generate kinetically stable membrane domains that give rise to coatomer-containing transport intermediates. In this model, unlike the sequential-binding model, coatomer exchange would continue even when vesicle formation is blocked.

Vesicular transport is known to be inhibited at temperatures below 15 °C and nonexistent at 4 °C (ref. 25). To evaluate the two models, we used FRAP to measure the kinetics of ϵCOP–GFP exchange between cytoplasmic and membrane pools at different temperatures. Both ϵCOP–GFP and Arf1–GFP were found to bind and release continuously from Golgi membranes at all temperatures down to 4 °C, with no abrupt change in the kinetics of these processes on reaching temperatures (that is, 15 °C) at which vesicle budding is slowed or inhibited[25] (Fig. 5c–e). At all temperatures, the release of ϵCOP–GFP from Golgi membranes was dependent on Arf1-GTP hydrolysis (not shown). The data thus indicate that the cycling of coatomer on and off membranes can be uncoupled from vesicle formation, and that feedback from productive vesicle budding is not necessary for coatomer dissociation.

On the basis of these findings, we favour the alternative model of coatomer activity with continuous membrane binding and release. Not only can it account for our observation that coatomer exhibits temperature-insensitive exponential release kinetics but it is consistent with other observations regarding the function and activity of coatomer. In the continuous binding and release model, coatomer, after being recruited by Arf1, could associate selectively with either protein or lipid species destined for transport[23,26], and coatomer–cargo complexes could cluster either because of direct inter-coatomer interactions or because of those induced via the mem-

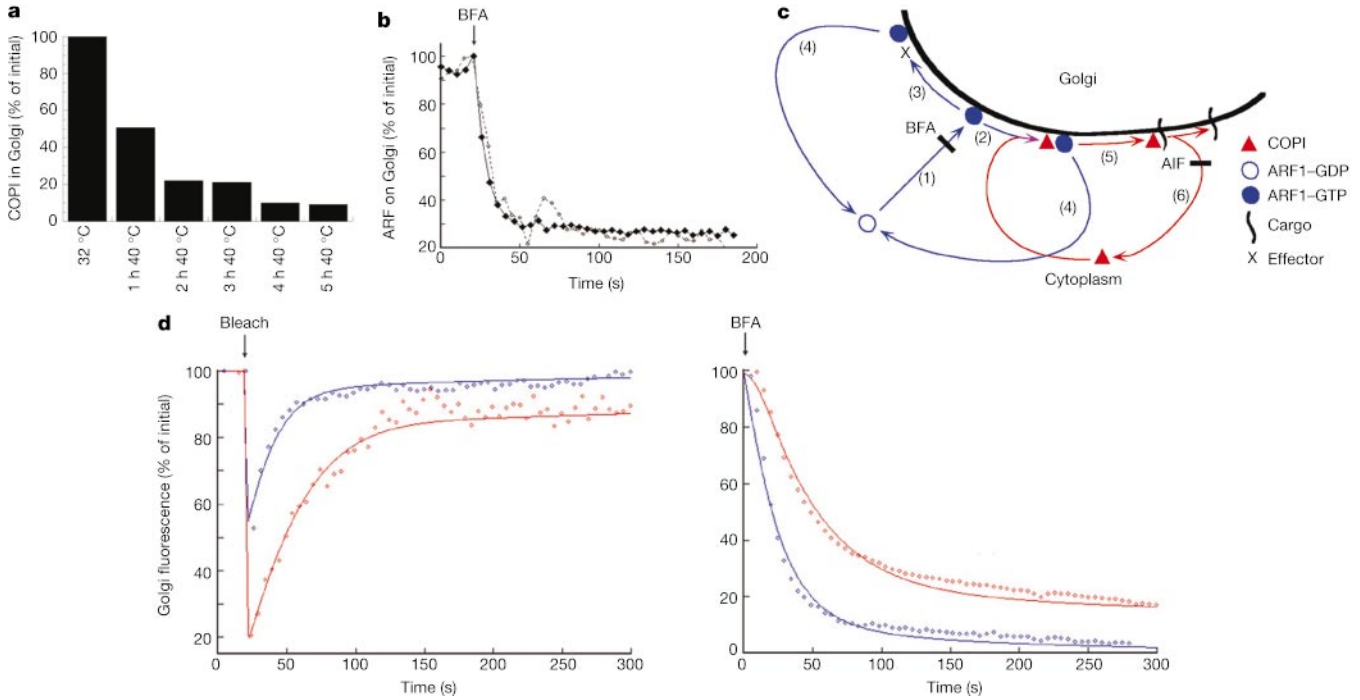

Figure 4 Kinetic modelling of coatomer and Arf1 activity and the effects of coatomer depletion on the rate of Arf1 dissociation from membranes. **a**, Conditions of coatomer depletion were determined by incubating, for increasing durations at 40 °C, *ldlF* cells that were not transfected with any protein. The amount of Golgi-associated COPI (visualized by antibody labelling with a rabbit anti-βCOP and a rhodamine anti-rabbit secondary antibody) was determined. Each time point is an average of Golgi-localized fluorescence per cell from 15 fields from 3 different coverslips. **b**, *ldlF* cells were transfected with Arf1–GFP and incubated at 32 °C (filled diamonds) or at 40 °C for 3 h (open circles) to deplete COPI from Golgi membranes. BFA was then added to inhibit the binding of Arf1 to membranes, and the release rate of Arf1–GFP fluorescence from Golgi was measured over time. **c**, Model of Arf1 and COPI membrane activity and turnover. **d**, Data sets from quantitative FRAP experiments measuring ϵCOP–GFP (red) and Arf1–GFP (blue) exchange on Golgi (see Supplementary Information) and the loss of ϵCOP–YFP (red) and Arf1–CFP (blue) from Golgi after the addition of BFA were simultaneously fitted to a mathematical formulation of the model shown in **c**. The smooth curves (red, COPI; blue, Arf1) represent the model solution obtained with parameter values (see the text) for the six processes in the model.

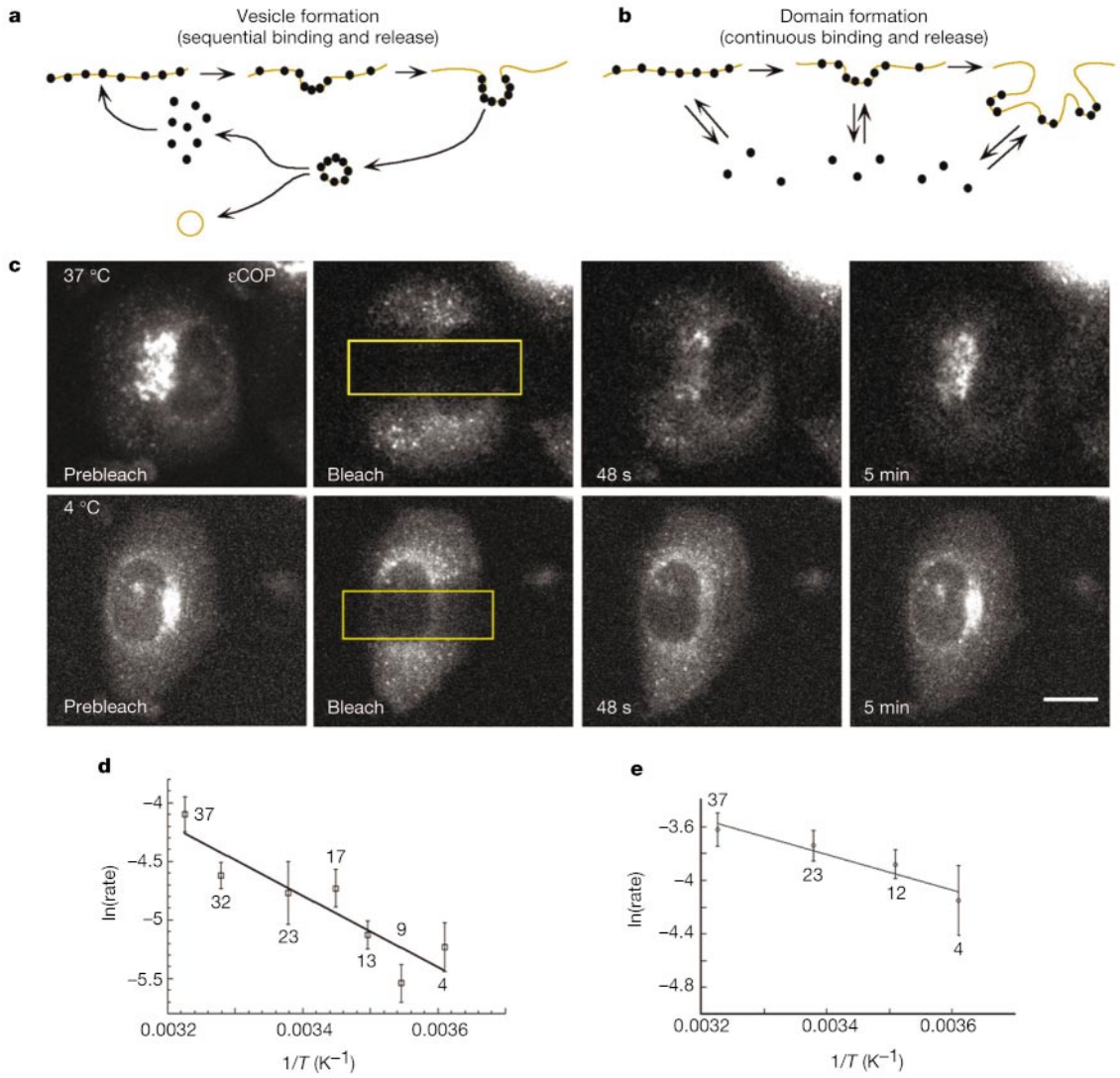

Figure 5 Testing different models of coatomer function on membranes. **a**, **b**, Two models for COPI function on Golgi membranes. In **a**, membrane binding and polymerization of COPI drives vesicle formation, with COPI dissociation from membranes occurring only after vesicle formation; in **b**, COPI binding and polymerization result in the formation of organized membrane domains that require continued binding and release of COPI to be maintained. **c**, FRAP of *ldlF* cell stably expressing ϵCOP–GFP on a microscope stage maintained at 37 °C or at 4 °C. Recovery of Golgi fluorescence in the bleached area (yellow box) occurred at both temperatures, indicating that membrane binding and release of COPI occurs even when vesicle budding and fusion are inhibited. Scale bar, 5 μM. (See Quicktime movies in Supplementary Information.) **d**, **e**, Arrhenius plots showing the effect of temperature on Golgi FRAP of ϵCOP–GFP in *ldlF* cells stably expressing ϵCOP–GFP (**d**) or in CHO cells transiently expressing Arf1–GFP (**e**). Numbers against points indicate temperatures in °C. The kinetics of recovery was fitted to a single-exponential curve and the mean rate coefficient was determined. Six to eight cells at each temperature were measured. The natural logarithm of the rate constant was then plotted against the reciprocal of the temperature in kelvins. Error bars indicate s.e.m.

branes. Continuing membrane binding and release of coatomer would allow the membrane at these sites to recruit cargo, alter their phospholipid composition and become larger, phase-separated domains (Fig. 5b). Accompanying these processes would be changes in membrane curvature and budding, which ultimately would transform the domains into either small coated vesicles[2] or larger transport intermediates[4,27]. Throughout the process of membrane transformation, coatomer would continually be recruited to membranes and then released into the cytosol. Because clusters of coatomer complexes in the differentiated membrane domains would be maintained by the Arf1–coatomer binding and release cycle, the domains could last longer than the 43 s residence time of an individual coatomer complex on membranes. Detachment of a transport intermediate from the coatomer-coated domain would therefore occur on a completely different timescale from that of the release of individual coatomer complexes, which correlates with topology changes underlying transport (that is, tubulation, fission and vesiculation) rather than uncoating.

Our observation that the activity of coatomer is not directly coupled to the formation of coated vesicles is consistent with recent FRAP data on the behaviour of clathrin, which has revealed large-scale exchange of clathrin even when clathrin-mediated endocytosis is inhibited[28]. Thus, coat proteins in general might undergo continuous exchange on and off membranes. As with coatomer, further investigation will help to determine whether this process is necessary to generate and maintain transport competent membrane domains, which could also function in membrane sorting and signalling. □

Methods

Cloning and expression of complementary DNAs

Arf1[Q71L], ϵCOP–GFP, ϵCOP–YFP, p58–CFP and VSVG–CFP plasmids were described

previously[13,29]. Arf1–CFP and Arf1–YFP were derived by the exchange of GFP for its spectral variant from Arf1–GFP[11]. DNAs were transiently transfected into cells by using FuGene 6 Transfection Reagent (Roche Molecular Biochemicals). Cell lines stably expressing ϵCOP–GFP and YFP were created by transient transfection followed by selection with G418, or in stably expressing *ldlF* cells selection was solely by ability to grow at 40 °C. Except where indicated, all experiments were performed in stable *ldlF* cell lines expressing ϵCOP–GFP/YFP at 40 °C, in *ldlF* cells transiently transfected with Arf1–GFP/CFP, and in wild-type Chinese hamster ovary (CHO) cells.

Fluorescence microscope systems, imaging and photobleaching analysis

Cells on coverslips or in LabTek chambers (Nalge Nunc) were imaged in buffered medium with a Zeiss 510 confocal microscope with a stage heated to 37 °C and fitted with an additional krypton laser with a 413-nm line for CFP/YFP double labelling or on a similarly configured Zeiss 410 confocal system. The time-lapse sequence shown in Fig. 1d and Fig. 1e was taken with a high-frame-rate spinning-disc confocal system, the Ultraview (lent by EG&G Wallac). Quantitative Golgi FRAP of ϵCOP–GFP was performed as described in Supplementary Information.

Received 2 November 2001; accepted 26 January 2002.

1. Schekman, R. & Orci, L. Coat proteins and vesicle budding. *Science* **271,** 1526–1533 (1996).
2. Rothman, J. E. & Wieland, F. T. Protein sorting by transport vesicles. *Science* **272,** 227–234 (1996).
3. Guo, Q., Penman, M., Trigatti, B. L. & Krieger, M. A single point mutation in ϵ-*COP* results in temperature-sensitive, lethal defects in membrane transport in a Chinese hamster ovary cell mutant. *J. Biol. Chem.* **271,** 11191–11196 (1996).
4. Presley, J. F. *et al.* ER-to-Golgi transport visualized in living cells. *Nature* **389,** 81–85 (1997).
5. Lahtinen, U., Dahllöf, B. & Saraste, J. Characterization of a 58 kDa *cis*-Golgi protein in pancreatic exocrine cells. *J. Cell Sci.* **103,** 321–333 (1992).
6. Shima, D. T., Scales, S. J., Kreis, T. E. & Pepperkok, R. Segregation of COPI-rich and anterograde-cargo-rich domains in endoplasmic-reticulum-to-Golgi transport complexes. *Curr. Biol.* **9,** 821–824 (1999).
7. Klumperman, J. *et al.* The recycling pathway of protein ERGIC-53 and dynamics of the ER-Golgi intermediate compartment. *J. Cell Sci.* **111,** 3411–3425 (1998).
8. Lippincott-Schwartz, J., Snapp, E. & Kenworthy, A. Studying protein dynamics in living cells. *Nature Rev. Mol. Cell Biol.* **2,** 444–456 (2001).
9. Dascher, C. & Balch, W. E. Dominant inhibitory mutants of ARF1 block endoplasmic reticulum to Golgi transport and trigger disassembly of the Golgi apparatus. *J. Biol. Chem.* **269,** 1437–1448 (1994).
10. Klausner, R. D., Donaldson, J. G. & Lippincott-Schwartz, J. Brefeldin A: Insights into the control of membrane traffic and organelle structure. *J. Cell Biol.* **116,** 1071–1080 (1992).
11. Vasudevan, C. *et al.* The distribution and translocation of the G protein ADP-ribosylation factor 1 in live cells is determined by its GTPase activity. *J. Cell Sci.* **111,** 1277–1285 (1998).
12. Peyroche, A. *et al.* Brefeldin A acts to stabilize an abortive ARF-GDP-Sec7 domain protein complex: Involvement of specific residues of the Sec7 domain. *Mol. Cell* **3,** 275–285 (1999).
13. Teal, S. B., Hsu, V. W., Peters, P. J., Klausner, R. D. & Donaldson, J. G. An activating mutation in ARF1 stabilizes coatomer binding to Golgi membranes. *J. Biol. Chem.* **269,** 3135–3138 (1994).
14. Goldberg, J. Decoding of sorting signals by coatomer through a GTPase switch in the COPI coat complex. *Cell* **100,** 671–679 (2000).
15. Szafer, E., Rotman, M. & Cassel, D. Regulation of GTP hydrolysis on ADP-ribosylation factor-1 at the Golgi membrane. *J. Biol. Chem.* **276,** 47834–47839 (2001).
16. Donaldson, J. G., Kahn, R. A., Lippincott-Schwartz, J. & Klausner, R. D. Binding of ARF and β-COP to Golgi membranes: possible regulation by a trimeric G protein. *Science* **254,** 1197–1199 (1991).
17. Kahn, R. A. Fluoride is not an activator of the smaller (20–25 kDa) GTP-binding proteins. *J. Biol. Chem.* **266,** 15595–15597 (1991).
18. Chardin, P. *et al.* A human exchange factor for ARF contains Sec7- and pleckstrin-homology domains. *Nature* **384,** 481–484 (1996).
19. Peyroche, A., Paris, S. & Jackson, C. L. Nucleotide exchange on ARF mediated by yeast Gea1 protein. *Nature* **384,** 479–481 (1996).
20. Zhao, L. *et al.* Direct and GTP-dependent interaction of ADP ribosylation factor 1 with coatomer subunit β. *Proc. Natl Acad. Sci. USA* **94,** 4418–4423 (1997).
21. Puertollano, R., Randazzo, P. A., Presley, J. F., Hartnell, L. M. & Bonifacino, J. S. The GGAs promote ARF-dependent recruitment of clathrin to the TGN. *Cell* **105,** 93–102 (2001).
22. Makler, V., Cukierman, E., Rotman, M., Admon, A. & Cassel, D. ADP-ribosylation factor-directed GTPase-activating protein. Purification and partial characterization. *J. Biol. Chem.* **270,** 5232–5237 (1995).
23. Sohn, K. *et al.* A major transmembrane protein of Golgi-derived COPI-coated vesicles involved in coatomer binding. *J. Cell Biol.* **135,** 1239–1248 (1996).
24. Lanoix, J. *et al.* GTP hydrolysis by arf-1 mediates sorting and concentration of Golgi resident enzymes into functional COP I vesicles. *EMBO J.* **18,** 4935–4948 (1999).
25. Bremser, M. *et al.* Coupling of coat assembly and vesicle budding to packaging of putative cargo receptors. *Cell* **96,** 495–506 (1999).
26. Cosson, P. & Letourneur, F. Coatomer interaction with di-lysine endoplasmic reticulum retention motifs. *Science* **263,** 1629–1631 (1994).
27. Lippincott-Schwartz, J., Roberts, T. H. & Hirschberg, K. Secretory protein trafficking and organelle dynamics in living cells. *Annu. Rev. Cell Dev. Biol.* **16,** 557–589 (2000).
28. Wu, X. *et al.* Clathrin exchange during clathrin-mediated endocytosis. *J. Cell Biol.* **155,** 291–300 (2001).
29. Ward, T. H., Polishchuk, R. S., Caplan, S., Hirschberg, K. & Lippincott-Schwartz, J. Maintenance of Golgi structure and function depends on the integrity of ER export. *J. Cell Biol.* **155,** 557–570 (2001).

Supplementary Information accompanies the paper on *Nature*'s website (http://www.nature.com).

Acknowledgements

We thank D. Hailey for help in the analysis of Arf1–GFP in yeast cells; M. Krieger for his gift of *ldlF* cells; F. Wieland and J. E. Rothman for ϵCOP cDNA; J. Donaldson for Arf1[Q71L] cDNA; G. Romero for the Arf1–GFP plasmid; EG&G Wallac for the use of their Ultravision spinning disc confocal system; and J. Donaldson, J. Bonifacino, C. Jackson, K. Hirschberg, B. Nichols, A. Kenworthy, N. Cole and H. Radhakrishna for valuable discussion. J.F.P. was supported in part by a grant from the Canadian Institutes of Health Research.

Competing interests statement

The authors declare that they have no competing financial interests.

Correspondence and requests for materials should be addressed to J. L. S. (e-mail: jlippin@helix.nih.gov).

Microtubule basis for left-handed helical growth in *Arabidopsis*

Siripong Thitamadee, Kazuko Tuchihara & Takashi Hashimoto

Graduate School of Biological Sciences, Nara Institute of Science and Technology, Takayama 8916-5, Ikoma 630-0101, Japan

Left–right asymmetry in plants can be found in helices of stalks, stems and tendrils, and in fan-like petal arrangements. The handedness in these asymmetric structures is often fixed in given species, indicating that genetic factors control asymmetric development[1]. Here we show that dominant negative mutations at the tubulin intradimer interface of α-tubulins 4 and 6 cause left-handed helical growth and clockwise twisting in elongating organs of *Arabidopsis thaliana*. We demonstrate that the mutant tubulins incorporate into microtubule polymers, producing right-handed obliquely oriented cortical arrays, in the root epidermal cells. The cortical microtubules in the mutants had increased sensitivity to microtubule-specific drugs. These results suggest that reduced microtubule stability can produce left-handed helical growth in plants.

Most twining plants, as they grow upward around sticks, trees, or other plants, coil in right-handed helices. Others coil the opposite way, and some exceptional species have genetically determined left- and right-handed varieties[1]. In contrast, the handedness of corolla contortion is either random in a species or fixed in a species or larger taxon. The fixed pattern mostly occurs in (but is not restricted to) the asterids, in which both clockwise and anticlockwise petal arrangements are seen in taxonomically loosely related groups[2]. Widespread distribution of helical structures with fixed handedness in diverse taxa implies that relatively small numbers of genes are responsible for the generation of such asymmetry.

Wild-type *Arabidopsis thaliana* axial organs do not twist during normal elongation growth and flowers are radially symmetrical (Fig. 1a, f, k). This symmetry can be broken, however, by mutations, including the right-handed helical growth mutants, *spiral1* (*spr1*) and *spr2* (ref. 3). In a search for suppressor mutants of the right-hand twisting mutant *spr1*, we identified two independent mutant loci, *lefty1* and *lefty2*. When outcrossed to remove the *spr1* mutation, both mutants display prominent left-handed helical growth phenotypes. The twisting phenotypes are somewhat stronger in *lefty2* than in *lefty1*. Petioles and petals of *lefty* mutants twist to give an appearance of clockwise bending when rosette leaves and flowers are viewed from above (Fig. 1g, h, l, m). The epidermal cell files of *lefty* hypocotyls and roots (Fig. 1q, r, t, u) form left-handed (S-form) helices, in contrast to straight wild-type cell files (Fig. 1p, s). The epidermal cell files of *lefty* roots begin to skew at the region where